Equivalence, Certified Convergence, and Blow-Up Analysis of a Sumudu–Sawi–Adomian Scheme for Nonlinear Goursat Problems

RAED R. ABU AWWAD[1], MONTHER AL-MOMANI[2], BAHA' ABUGHAZALEH[3,*]

[1]Department of Mathematics, University of Petra, Amman
JORDAN

[2]Department of Mathematics, Amman Arab University, Amman
JORDAN

[3]Department of Mathematics, Isra University, Amman
JORDAN

[*]*Corresponding Author*

Abstract: The double Sumudu–Sawi transform reduces to the double Laplace transform by rescaling. On a finite rectangle the Goursat problem takes Volterra form. An invariant ball on which the integral map contracts gives existence and uniqueness within that ball. Analytic dependence on the embedding parameter gives convergence and a geometric tail bound for the Adomian series. We obtain two-sided residual bounds and account for product trapezoidal quadrature separately from iteration error. An explicit family has a series that converges for $0 \le xt < 1$ and a solution that blows up at $xt = 1$. Padé approximation recovers the rational members exactly. The numerical examples cover a manufactured solution, a problem without a known closed form and a coupled system. Residuals can fall below the quadrature error floor. Grid refinement shows second-order self-convergence. The bounds hold in exact arithmetic.

Key-Words: Adomian decomposition; Goursat problem; double Sumudu–Sawi transform; Volterra equation; residual estimate; blow-up; Padé approximation.

MSC 2020: 35A01, 35A02, 35B40, 44A10, 45D05.

Received: May 27, 2026. Revised: August 2, 2026. Accepted: September 4, 2026. Published: November 26, 2026.

1 Introduction

Convergence of the Adomian decomposition method (ADM) is studied, [1], [2], [3]. An analysis of convergence for initial-value problems is available, [4]. Several recurrences compute the multivariable Adomian polynomials, [5], [6]. Other work addresses how to accelerate the series, [7], and how to use decomposition for nonlinear systems, [8].

The Sumudu transform was introduced as a tool for differential equations, [9]. The Sawi transform and its applications to differential equations are described, [10], [11]. Examples of mixed transforms formed from one-variable kernels are the double Mellin–ARA and double ARA–Sawi transforms, [12], [13]. The scaling identity below relates the Sumudu–Sawi kernel to the double Laplace transform.

On $\Omega = [0, X] \times [0, T]$, we consider the nonlinear Goursat problem

$$u_{xt}(x,t) = f(x,t) + au(x,t) + N(u(x,t)), \quad (1)$$

$$u(x,0) = \phi(x), \quad u(0,t) = \psi(t), \quad (2)$$

$$\phi(0) = \psi(0) = u_c. \quad (3)$$

Direct integration of the mixed derivative gives the Volterra equation on the rectangle. The normalization of the double Sumudu–Sawi kernel accounts for its scaling relative to the double Laplace transform.

We use a real invariant ball to study solvability and a complex embedding parameter to estimate the ADM tail by Cauchy's formula. The nonlinear test family gives the full coefficient sequence and an exact convergence boundary. It also supplies cases where the local series converges and the global transform fails.

For the numerical tests we compare ADM with Picard iteration on a common grid. Related work treats collocation in two dimensions and spectral methods for multidimensional nonlinear equations, [14], [15]. Discretization and extrapolation also appear in two-dimensional nonlinear Volterra–Urysohn problems, [16]. Here the residual estimates separate error in the discrete iteration from error in the product quadrature. This distinction matters when the discrete residual keeps falling after the error against the continuous solution has levelled off.

2 Transform identity and direct Volterra reduction

Applying the Sumudu kernel in x and the Sawi kernel in t gives the following product transform for $\xi, \eta > 0$ whenever the integral converges

$$\mathscr{T}_{DSW}[v](\xi,\eta) := \frac{1}{\xi\eta^2} \int_0^\infty \int_0^\infty e^{-x/\xi - t/\eta} v(x,t)\, dt\, dx. \quad (4)$$

Let $\mathcal{L}_2[v](p,q) = \int_0^\infty \int_0^\infty e^{-px-qt} v(x,t)\, dt\, dx$ be the ordinary double Laplace transform.

Theorem 2.1 (Collapse of the transform)**.** *Whenever either side exists absolutely,*

$$\mathscr{T}_{DSW}[v](\xi,\eta) = \frac{1}{\xi\eta^2}\mathcal{L}_2[v]\left(\frac{1}{\xi},\frac{1}{\eta}\right). \qquad (5)$$

Consequently, the double Sumudu–Sawi transform contains no parameter that is independent of the two Laplace frequencies.

Proof. Substitution of $p = 1/\xi$ and $q = 1/\eta$ in the definition of $\mathcal{L}_2$ gives (5); the remaining factor is the normalization in (4). Absolute convergence permits the order of integration used in both definitions. □

For $g \in C(\Omega)$, introduce the Volterra operator

$$(\mathcal{J}g)(x,t) := \int_0^x \int_0^t g(r,s)\, ds\, dr \qquad (6)$$

and set

$$b(x,t) := \phi(x) + \psi(t) - u_c + \mathcal{J}f(x,t). \qquad (7)$$

Direct integration with (6) and the boundary term in (7) gives

$$u = \Phi(u), \qquad \Phi(v) := b + \mathcal{J}\{av + N(v)\}. \qquad (8)$$

The next proposition establishes the equivalence.

Proposition 2.2 (Direct equivalence)**.** *Assume f is continuous, $\phi \in C^1[0,X]$, $\psi \in C^1[0,T]$, the compatibility condition in* (3) *holds, and N is continuous. Here a classical solution has continuous first derivatives and continuous mixed derivative u_{xt}. A classical solution of* (1) *with data* (2)–(3) *satisfies* (8)*. A continuous fixed point of* (8) *has the regularity of a classical solution of* (1)–(3) *under the same hypotheses. With compatible traces that are only continuous, the integral equation defines the mild formulation.*

Proof. Integrating u_{xt} first over $[0,t]$ and then over $[0,x]$ gives

$$\mathcal{J}u_{xt} = u(x,t) - u(x,0) - u(0,t) + u(0,0). \qquad (9)$$

Substituting (2) and (3) into (9) yields (8). On the edges $t = 0$ and $x = 0$ the integral in (8) vanishes, leaving the prescribed traces. Taking the mixed derivative and using $(\mathcal{J}g)_{xt} = g$ gives (1). □

Remark 2.3. Theorem 2.1 identifies the Sumudu–Sawi notation as a rescaling of two Laplace frequencies. Any computational benefit comes from the Volterra reduction or the decomposition and continuation procedures.

3 Decomposition, convergence, and residual control

Let $E = C(\Omega)$ with $\|v\|_\infty = \max_\Omega |v|$ and let $B_M = \{v \in E : \|v\|_\infty \le M\}$. Assume that N is Lipschitz on $[-M,M]$ with constant L_M, and put

$$C_M := \max_{|z|\le M} |N(z)|, \qquad q := XT\big(|a| + L_M\big). \qquad (10)$$

Theorem 3.1 (Solvability)**.** *With C_M and q as in* (10)*, suppose*

$$\|b\|_\infty + XT\big(|a|M + C_M\big) \le M, \qquad q < 1, \quad (11)$$

then (8) *has a unique solution in B_M.*

Proof. Since $\|\mathcal{J}g\|_\infty \le XT\,\|g\|_\infty$, the first inequality in (11) gives $\Phi(B_M) \subseteq B_M$. For $v, w \in B_M$,

$$\begin{aligned}\|\Phi(v) - \Phi(w)\|_\infty &\le XT(|a| + L_M)\,\|v - w\|_\infty \\ &= q\,\|v - w\|_\infty .\end{aligned} \qquad (12)$$

The ball B_M is closed in the Banach space $C(\Omega)$ and is therefore complete. The contraction estimate (12) allows Banach's theorem to apply. It gives a fixed point in this ball and convergence of every Picard sequence started there. If $u, v \in B_M$ are fixed points then $\|u - v\|_\infty \le q\,\|u - v\|_\infty$, which proves uniqueness within the ball. These inequalities are sufficient conditions and need not hold on every rectangle where a solution exists. □

Introduce the embedding parameter p to specify the decomposition.

$$u(p) = b + p\mathcal{J}\{au(p) + N(u(p))\}. \qquad (13)$$

In (13), write $u(p) = \sum_{n\ge0} u_n p^n$ and

$$N\left(\sum_{n\ge0} u_n p^n\right) = \sum_{n\ge0} A_n p^n, \qquad (14)$$

$$A_n = \frac{1}{n!}\,\frac{d^n}{dp^n} N\left(\sum_{j\ge0} u_j p^j\right)\Bigg|_{p=0}. \qquad (15)$$

A computational form of the Adomian polynomials is given in the literature, [17]. Comparing coefficients using (14) and (15) gives the recurrence

$$u_0 = b, \qquad u_{n+1} = \mathcal{J}(au_n + A_n), \quad n \ge 0. \quad (16)$$

The contraction argument gives convergence of Picard iteration. Convergence of the ADM series follows from the additional analyticity conditions below.

Theorem 3.2 (ADM convergence with a tail bound)**.** *Suppose N has a holomorphic extension to a complex*

neighbourhood of the closed disk $|z| \le M$. *If there is an* $R > 1$ *such that*

$$\|b\|_\infty + RXT(|a|M + C_M) \le M, \tag{17}$$
$$RXT(|a| + L_M) < 1, \tag{18}$$

where C_M *and* L_M *are valid on the complex disk, then the series generated by* (16) *converges uniformly at* $p = 1$ *to the unique solution of* (8)*. Moreover,*

$$\|u_n\|_\infty \le MR^{-n},$$
$$\left\| u - \sum_{j=0}^{n} u_j \right\|_\infty \le \frac{MR^{-(n+1)}}{1 - R^{-1}}. \tag{19}$$

Proof. For fixed p with $|p| \le R$, define $\Phi_p(v) = b + p\mathcal{J}(av + N(v))$ on the complexification of B_M. Conditions (17)–(18) make Φ_p a uniform strict contraction of this ball into itself. Starting with b, its Picard iterates are holomorphic in p and converge uniformly for $|p| \le R$. The nonlinear composition is holomorphic because N is holomorphic on a neighbourhood of the value disk. The limit $u(p)$ is holomorphic for $|p| < R$ and has norm at most M. For each $r < R$, its Banach-space Cauchy integral gives $\|u_n\|_\infty \le Mr^{-n}$. Letting $r \uparrow R$ proves the coefficient bound without assuming analyticity across the boundary $|p| = R$. Near $p = 0$ the normally convergent series can be substituted into N. Coefficient comparison then gives (16). Since $R > 1$, this series converges absolutely in $C(\Omega)$ at $p = 1$. Summing its geometric majorant proves (19). □

In this theorem one may take $C_M = \max_{|z|\le M} |N(z)|$ and $L_M = \max_{|z|\le M} |N'(z)|$ over complex z. The segment joining two points of the disk stays inside it, so integration of N' along that segment gives the required Lipschitz estimate. Real-axis bounds alone do not establish (18).

The bound (19) is an a priori estimate. A computed approximation can be checked more sharply through its fixed-point defect.

Theorem 3.3 (Residual certificate)**.** *Under the assumptions of Theorem 3.1, let* u *be the fixed point and let* $w \in B_M$ *with* $\Phi(w) \in B_M$*. Then*

$$\frac{\mathrm{Res}(w)}{1+q} \le \|u - w\|_\infty \le \frac{\mathrm{Res}(w)}{1-q}, \qquad \mathrm{Res}(w) := \|w - \Phi(w)\|_\infty. \tag{20}$$

Proof. The identity $u = \Phi(u)$ and the contraction estimate yield

$$\|u - w\|_\infty \le \|\Phi(u) - \Phi(w)\|_\infty + \|\Phi(w) - w\|_\infty \le q\,\|u - w\|_\infty + \mathrm{Res}(w). \tag{21}$$

Rearranging (21) proves the upper bound in (20). For the lower bound use $\mathrm{Res}(w) \le \|w - u\|_\infty + \|\Phi(u) - \Phi(w)\|_\infty \le (1 + q)\,\|w - u\|_\infty$. Ball invariance already implies $\Phi(w) \in B_M$. □

For systems, take the maximum norm over the components. If the Jacobian of the nonlinear vector field is bounded by L_M in the induced maximum norm, Theorems 3.1 and 3.3 remain valid with the same proof.

4 A blow-up family and the exact boundary of the series

Consider, for $\kappa > 0$,

$$u_{xt} = \kappa(\kappa + 1)u^{1+2/\kappa} - \kappa^2 u^{1+1/\kappa}, \tag{22}$$
$$u(x, 0) = u(0, t) = 1. \tag{23}$$

This is a genuine mixed-derivative equation; both variables enter the nonlinearity through the solution.

Proposition 4.1 (Exact decomposition and blow-up)**.** *For the homotopy obtained by multiplying the right-hand side of* (22) *by* p*, the analytic solution near* $p = 0$ *is*

$$u(p, x, t) = (1 - pxt)^{-\kappa}. \tag{24}$$

Consequently, ADM produces

$$u_n(x, t) = \frac{(\kappa)_n}{n!}(xt)^n, \tag{25}$$

where $(\kappa)_0 = 1$ *and* $(\kappa)_n = \kappa(\kappa+1)\cdots(\kappa+n-1)$*. For* $x, t \ge 0$ *at* $p = 1$ *the series converges precisely for* $xt < 1$*. It converges uniformly on every rectangle with* $XT < 1$*. The positive solution* $u = (1 - xt)^{-\kappa}$ *blows up as* $xt \uparrow 1$*.*

Proof. Choose the branch that equals one at $p = 0$. For $|pxt| < 1$,

$$\begin{aligned} u_x &= \kappa pt(1 - pxt)^{-\kappa-1}, \\ u_{xt} &= \kappa p(1 - pxt)^{-\kappa-1} \\ &\quad + \kappa(\kappa + 1)p^2 xt(1 - pxt)^{-\kappa-2} \\ &= p\kappa(1 - pxt)^{-\kappa-2}(1 + \kappa pxt). \end{aligned} \tag{26}$$

On the other hand, substituting (24) into the right-hand side of (22) and multiplying by p gives the mixed derivative in (26). The solution also satisfies (23). Near $p = 0$, contraction on a ball around the constant function one identifies this analytic solution. With $z = pxt$ and $F(z) = (1 - z)^{-\kappa}$, the identity $(1 - z)F' = \kappa F$ gives

$$c_0 = 1, \qquad c_{n+1} = \frac{n + \kappa}{n + 1}c_n, \qquad c_n = \frac{(\kappa)_n}{n!}. \tag{27}$$

The recurrence (27) gives the ADM coefficients in (25). The ratio test gives radius one in z. At $z = 1$ the positive partial sums diverge because $F(z) \to \infty$ as $z \uparrow 1$. For $z > 1$ the terms do not tend to zero. Uniform convergence for $XT < 1$ follows by comparison with $\sum c_n(XT)^n$. The branch is positive on $xt < 1$ and has the stated blow-up limit.

Uniqueness of this positive solution on a compact rectangle with $XT < 1$ does not require the smallness condition (11). For two bounded positive solutions the nonlinearity is Lipschitz on their common range. Their difference satisfies $|d| \le L\mathcal{J}|d|$. Iteration gives $|d(x,t)| \le \|d\|_\infty L^m x^m t^m/(m!)^2$ for every m. Its right-hand side tends to zero. □

The stated convergence boundary is for the nonnegative quadrant. For $0 < \kappa < 1$ the point $z = -1$ gives conditional convergence on $|z| = 1$.

For $\kappa = 1$, equation (22) becomes $u_{xt} = 2u^3 - u^2$ and $u = (1 - xt)^{-1}$. The raw truncation error is exactly

$$E_n(z) = \frac{z^{n+1}}{1-z}, \qquad z = xt \in [0,1). \tag{28}$$

For a positive integer κ the algebraic Padé construction, [18], uses the first $\kappa + 1$ coefficients for the $[0/\kappa]$ approximant. It recovers (24) exactly as a rational function. The power series still has its boundary at $|xt| = 1$.

Remark 4.2 (Why the global transform fails). Fix $x > 0$ and take $\kappa \ge 1$. The exponential weight has a positive lower bound near $t = 1/x$. On the approach to the singularity the inner integral is bounded below by a positive constant times $\int_0^\varepsilon r^{-\kappa}\,dr$, which diverges. Tonelli's theorem gives divergence of the absolute double integral. This includes the rational cases $\kappa = 1, 2$. For $0 < \kappa < 1$ the same local integral is finite, leaving global transform convergence open. The positive classical branch reaches its endpoint at $xt = 1$. A continuation would require a branch choice and a different interpretation of the solution.

The geometric series converges more slowly near the singular curve as seen in Figure 1 (Appendix) and Table 1 (Appendix). For $\kappa = 1$ the Padé approximation gives the exact rational value and retains the pole. Each curve in Figure 1 (Appendix) shows the absolute error (28) for a fixed z with $n+1$ terms retained. For an increment d in the index, $E_{n+d}/E_n = z^d$. Thus the curve flattens as $z \uparrow 1$, while the factor $(1-z)^{-1}$ increases its height. The relative error is z^{n+1}. The coefficients $c_0 = c_1 = 1$ give this exact Padé result. It is not evidence of stable continuation from noisy coefficients near the pole and it does not regularize the blow-up.

5 Computational realization and numerical tests

Quadrature and piecewise-polynomial methods for Volterra equations provide background for this discretization, [19], [20]. On a tensor grid, $\mathcal{J}$ is approximated by successive cumulative trapezoidal rules in t and x. All nonlinear products are evaluated pointwise. The discrete defect uses the same quadrature operator as the iteration, while comparison with an exact solution also contains quadrature error. The reported calculations were performed in MATLAB on a 401×401 grid unless a grid size is displayed explicitly. The accompanying file `verify_dsw_adm.m` reproduces every value in this section.

Write $x_i = ih_x$ and $t_j = jh_t$ with $h_x = X/N_x$ and $h_t = T/N_t$. There are $(N_x+1)(N_t+1)$ grid nodes. For $i, j \ge 1$ the rule is

$$(\mathcal{J}_h G)_{ij} = h_x h_t \sum_{k=0}^{i}\sum_{\ell=0}^{j} \omega_k^{(i)}\omega_\ell^{(j)} G_{k\ell}, \tag{29}$$

where the endpoint weights are $1/2$ and the interior weights are one. The value is zero on either boundary axis. Set $b_h = \phi_h + \psi_h - u_c + \mathcal{J}_h f_h$ and $\Phi_h(W) = b_h + \mathcal{J}_h(aW + N(W))$. The reported measures are

$$\begin{aligned} \|W\|_{\infty,h} &= \max_{i,j} |W_{ij}|, \\ r_h(W) = \mathrm{Res}_h(W) &= \|W - \Phi_h(W)\|_{\infty,h}\,. \end{aligned} \tag{30}$$

For systems the maximum also runs over the components. The index n denotes the partial sum $S_n = \sum_{j=0}^{n} u_{j,h}$ or n Picard updates from b_h. It is not a mesh refinement index.

Proposition 5.1 (Discrete residual and consistency)**.** *Suppose $q < 1$ and $\|b_h\|_{\infty,h} + XT(|a|M + C_M) \le M$. Then Φ_h has a unique fixed point u_h in the grid ball of radius M. Every W in this ball satisfies*

$$\frac{r_h(W)}{1+q} \le \|W - u_h\|_{\infty,h} \le \frac{r_h(W)}{1-q}. \tag{31}$$

If a continuous solution $u \in B_M$ also exists and $g = f + au + N(u)$ has continuous second derivatives in each variable, then

$$\|W - u|_h\|_{\infty,h} \le \frac{r_h(W) + \delta_h}{1-q}, \tag{32}$$

where a valid consistency bound is

$$\delta_h = \frac{XT}{12}\left(h_x^2\,\|g_{xx}\|_\infty + h_t^2\,\|g_{tt}\|_\infty\right). \tag{33}$$

Proof. The nonnegative weights in (29) sum to $x_i t_j \le XT$. Thus $\|\mathcal{J}_h\| \le XT$ and the ball and contraction estimates are the same as in Theorem 3.1. The proof of Theorem 3.3 gives (31). Applying the one-dimensional composite trapezoidal error bound in each variable gives $\|(\mathcal{J}g)|_h - \mathcal{J}_h(g|_h)\|_{\infty,h} \le \delta_h$. The continuous integral equation therefore implies $\|u|_h - \Phi_h(u|_h)\|_{\infty,h} \le \delta_h$. Adding and subtracting $\Phi_h(W)$ and using the contraction estimate proves (32). □

Only the first term in (32) is determined by the computed residual. The consistency bound (33) requires derivative bounds for the continuous solution. A vanishing r_h alone does not certify

the continuous error. The estimates use exact arithmetic. The double-precision implementation uses no rounding-error enclosure. It checks the change between successive Picard iterates against 10^{-14}, with 2×10^{-14} used for the refinement runs. The code checks convergence and saves the final defect.

5.1 Smooth transform-compatible problem

Take $X = T = 1/2$ and

$$\begin{aligned} u_{xt} &= e^{x+t} - e^{2x+2t} + u^2, \\ u(x,0) &= e^x, \quad u(0,t) = e^t. \end{aligned} \tag{34}$$

For $u = e^{x+t}$ the transform exists at sufficiently large Laplace frequencies. Here $a = 0$ and $N(u) = u^2$, with $b = e^x + e^t - 1 + \mathcal{J}(e^{x+t} - e^{2x+2t})$. Squaring the series gives $A_n = \sum_{j=0}^{n} u_j u_{n-j}$. The grid error and residual in Table 2 are maxima over the nodes of $[0, 1/2]^2$. They fall at comparable rates until the quadrature contribution becomes appreciable. At $n = 6$ they are 4.86×10^{-6} and 4.93×10^{-6} respectively. This table illustrates convergence but is not an application of the unweighted certificate: every ball containing $u = e^{x+t}$ has $M \geq e$ and hence $q = M/2 > 1$. The sufficient condition in Theorem 3.1 fails on this rectangle even though the exact solution exists.

Table 2. ADM results for the smooth manufactured problem (34).

n	$\|S_n - u\|_{\infty,h}$	$\mathrm{Res}_h(S_n)$
0	7.381238×10^{-1}	6.161090×10^{-1}
1	1.220148×10^{-1}	1.113883×10^{-1}
2	1.792717×10^{-2}	1.698692×10^{-2}
3	2.444541×10^{-3}	2.359289×10^{-3}
4	3.188344×10^{-4}	3.110195×10^{-4}
5	4.023944×10^{-5}	3.962008×10^{-5}
6	4.864758×10^{-6}	4.927058×10^{-6}

Source: created by the authors.

5.2 Problem without a known closed form: ADM versus Picard

On $[0, 1/4]^2$, consider

$$\begin{aligned} u_{xt} &= x + t + \tfrac{1}{2}u + u^3, \\ u(x,0) &= x, \quad u(0,t) = t. \end{aligned} \tag{35}$$

Thus $b = x + t + \frac{1}{2}x^2 t + \frac{1}{2}xt^2$. For $M = 1$, $\|b\|_\infty = 0.515625$, the ball-invariance bound is $0.609375 < 1$, and the contraction constant is $q = (1/16)(1/2+3) = 0.21875$. Choosing $R = 2$ also satisfies (17)–(18), so Theorem 3.2 applies and gives the conservative bound $\|u - S_n\|_\infty \leq 2^{-n}$. Indeed the complex ball bound at $R = 2$ is 0.703125 and $Rq = 0.4375$.

For u^3, the Adomian polynomial is $A_n = \sum_{i+j+k=n} u_i u_j u_k$. A converged discrete Picard solution is used only as a numerical reference. Both columns in Table 3 (Appendix) converge to the same discrete value. In this particular calculation, the Picard error begins to fall more rapidly after iteration two. The example therefore gives no basis for treating ADM as uniformly faster. The error columns use the maximum difference from the converged grid reference. The residual columns use (30) and do not use that reference. For example the ADM residual at $n = 2$ gives an upper grid-error bound of 9.42×10^{-7} through (31), compared with the observed 7.37×10^{-7}. Values at machine precision indicate agreement between the stored arrays. The zero in the Picard column measures agreement with the discrete reference. Quadrature error can still separate that reference from the continuous solution.

Table 4 measures refinement through the corner value. The continuous solution is unknown. Successive differences decrease by a factor of four, giving the expected second-order rate of the product trapezoidal rule. The first column gives the subinterval count per coordinate. If c_N is the computed corner value, the difference is $d_N = |c_N - c_{N/2}|$ and the reported order is $\log_2(d_{N/2}/d_N)$. These values demonstrate nodal self-convergence rather than a measured error against an exact solution. The asymptotic estimate $d_{800}/3 \approx 1.91 \times 10^{-9}$ is a Richardson estimate at the finest corner and is not a rigorous error bound.

Table 4. Grid self-convergence for (35).

$N_x = N_t$	$u_h(0.25, 0.25)$	refinement difference	order
50	0.525132678502	–	–
100	0.525132310897	3.676056×10^{-7}	–
200	0.525132218997	9.189993×10^{-8}	2.000
400	0.525132196022	2.297489×10^{-8}	2.000
800	0.525132190278	5.743717×10^{-9}	2.000

Source: created by the authors.

5.3 Coupled nonlinear system

To test the vector extension, let $X = T = 1/4$ and consider

$$u_{xt} = e^{x+t} - e^{2x} + uv, \tag{36}$$

$$v_{xt} = -e^{x-t} - e^{2x+2t} + u^2, \tag{37}$$

with

$$\begin{aligned} u(x,0) &= e^x, \quad u(0,t) = e^t, \\ v(x,0) &= e^x, \quad v(0,t) = e^{-t}. \end{aligned} \tag{38}$$

The exact pair satisfying (36)–(37) and (38) is $(u, v) = (e^{x+t}, e^{x-t})$. For the coefficient of degree n, the two nonlinear polynomials are $\sum_{j=0}^{n} u_j v_{n-j}$ and $\sum_{j=0}^{n} u_j u_{n-j}$. Table 5 shows that the iteration residual continues to fall after the true error has

reached the 5.2×10^{-9} quadrature floor. This is precisely why iteration and discretization errors should not be reported as if they were the same quantity. For this system $\|(u, v)\|_\infty \leq e^{1/2} < 2$. On the componentwise ball with $M = 2$, the nonlinear map (uv, u^2) has $C_M = 4$ and Jacobian row-sum bound $L_M = 4$, so $q = 1/4$. The two components of b are $e^{x+t} - t(e^{2x} - 1)/2$ and $e^{x-t} - (e^{2x} - 1)(e^{2t} - 1)/4$. They are positive on this rectangle and $\|b\|_\infty \leq e^{1/2}$. Consequently $\|b\|_\infty + XTC_M < 1.899 < 2$. The same estimate with $R = 1.2$ is below 1.949 and $Rq = 0.3$. Thus both continuous theorems apply. The code checks the corresponding discrete ball bound. The residual certifies convergence to the discrete solution while the error column still contains quadrature error.

Figure 2 (Appendix) plots $r_h(S_n)$ on a logarithmic vertical axis. Each term lowers the smooth scalar residual by about a factor of ten. The cubic test on the smaller domain reaches roundoff after about six terms. The coupled residual continues to fall below the true-error floor of 5.2×10^{-9}. The smaller boundary values and integration area in the cubic test help explain its faster decay relative to the smooth scalar test. At residuals near 10^{-15} the curves are sensitive to roundoff, which limits the accuracy of the error estimates.

Table 5. Largest componentwise error and residual in the coupled system (36)–(37).

n	vector error	vector residual
0	1.052099×10^{-1}	1.019843×10^{-1}
1	3.225551×10^{-3}	3.169918×10^{-3}
2	9.499752×10^{-5}	9.417533×10^{-5}
3	2.682375×10^{-6}	2.672578×10^{-6}
4	7.459185×10^{-8}	7.188928×10^{-8}
5	5.725168×10^{-9}	1.868940×10^{-9}
6	5.192519×10^{-9}	4.747390×10^{-11}

Source: created by the authors.

6 Conclusion

The double Sumudu–Sawi transform and the double Laplace transform are equivalent under rescaling. On a finite rectangle direct integration gives the same Volterra problem. Its fixed point is unique in the invariant ball under the contraction condition. Analyticity gives a geometric ADM tail bound, and the residual estimates the error of a finite sum.

For the rational benchmarks the coefficient sequence gives convergence for $|xt| < 1$. The pole at $xt = 1$ prevents a global transform on the positive quadrant. Padé approximation recovers the rational function with its pole.

On the grid the residual continues to measure iteration error even when quadrature limits accuracy against the continuous solution. Successive refinements show the second-order rate of the product trapezoidal rule. The contraction estimates use the stated Lipschitz and kernel assumptions. Non-Lipschitz nonlinearities and weakly singular two-dimensional kernels call for a separate analysis.

Declaration of Generative AI and AI-assisted Technologies in the Writing Process

During the preparation of this work, the author(s) utilized artificial intelligence (AI) technologies solely for the purpose of linguistic refinement and grammatical correction. Following the application of these tools, the author(s) comprehensively reviewed, verified, and edited the resulting text. The author(s) maintain full accountability and responsibility for the accuracy, integrity, and final content of the publication.

References:

[1] Y. Cherruault, Convergence of Adomian's method, *Kybernetes*, Vol. 18, No. 2, 1989, pp. 31–38. https://doi.org/10.1108/eb005812.

[2] K. Abbaoui and Y. Cherruault, Convergence of Adomian's method applied to differential equations, *Computers & Mathematics with Applications*, Vol. 28, No. 5, 1994, pp. 103–109. https://doi.org/10.1016/0898-1221(94)00144-8.

[3] Y. Cherruault, G. Adomian, K. Abbaoui, and R. Rach, Further remarks on convergence of decomposition method, *International Journal of Bio-Medical Computing*, Vol. 38, No. 1, 1995, pp. 89–93. https://doi.org/10.1016/0020-7101(94)01042-Y.

[4] A. Abdelrazec and D. Pelinovsky, Convergence of the Adomian decomposition method for initial-value problems, *Numerical Methods for Partial Differential Equations*, Vol. 27, No. 4, 2011, pp. 749–766. https://doi.org/10.1002/num.20549.

[5] J.-S. Duan, An efficient algorithm for the multivariable Adomian polynomials, *Applied Mathematics and Computation*, Vol. 217, No. 6, 2010, pp. 2456–2467. https://doi.org/10.1016/j.amc.2010.07.046.

[6] J.-S. Duan, Convenient analytic recurrence algorithms for the Adomian polynomials, *Applied Mathematics and Computation*, Vol. 217, No. 13, 2011, pp. 6337–6348. https://doi.org/10.1016/j.amc.2011.01.007.

[7] M. Turkyilmazoglu, Accelerating the convergence of Adomian decomposition method (ADM), *Journal of Computational Science*, Vol. 31, 2019, pp. 54–59. https://doi.org/10.1016/j.jocs.2018.12.014.

[8] W. Li and Y. Pang, Application of Adomian decomposition method to nonlinear systems, *Advances in Difference Equations*, Vol. 2020, No. 1, 2020, Article 67. https://doi.org/10.1186/s13662-020-2529-y.

[9] G. K. Watugala, Sumudu transform: a new integral transform to solve differential equations and control engineering problems, *International Journal of Mathematical Education in Science and Technology*, Vol. 24, No. 1, 1993, pp. 35–43. https://doi.org/10.1080/0020739930240105.

[10] M. M. A. Mahgoub, The new integral transform "Sawi Transform", *Advances in Theoretical and Applied Mathematics*, Vol. 14, No. 1, 2019, pp. 81–87. https://www.ripublication.com/atam19/atamv14n1_05.pdf (Accessed Date: November 12, 2026).

[11] M. Higazy and S. Aggarwal, Sawi transformation for system of ordinary differential equations with application, *Ain Shams Engineering Journal*, Vol. 12, No. 3, 2021, pp. 3173–3182. https://doi.org/10.1016/j.asej.2021.01.027.

[12] B. Abughazaleh, M. A. Amleh, A. Al-Natoor, and R. Saadeh, Double Mellin-ARA Transform, in A. Burqan, R. Saadeh, A. Qazza, O. Y. Ababneh, J. C. Cortés, K. Diethelm, and D. Zeidan (eds.), *Mathematical Analysis and Numerical Methods: IACMC 2023*, Zarqa, Jordan, May 10–12, 2023, Springer Proceedings in Mathematics & Statistics, Vol. 466, Springer, Singapore, 2024, pp. 383–394. https://doi.org/10.1007/978-981-97-4876-1_26.

[13] R. R. Abu Awwad, M. Al-Momani, A. Jaradat, B. Abughazaleh, and A. Al-Natoor, The Double ARA-Sawi Transform, *European Journal of Pure and Applied Mathematics*, Vol. 18, No. 1, 2025, Article 5807. https://doi.org/10.29020/nybg.ejpam.v18i1.5807.

[14] H. Brunner and J.-P. Kauthen, The numerical solution of two-dimensional Volterra integral equations by collocation and iterated collocation, *IMA Journal of Numerical Analysis*, Vol. 9, No. 1, 1989, pp. 47–59. https://doi.org/10.1093/imanum/9.1.47.

[15] Y. Wei, Y. Chen, X. Shi, and Y. Zhang, Jacobi spectral collocation method for the approximate solution of multidimensional nonlinear Volterra integral equation, *SpringerPlus*, Vol. 5, No. 1, 2016, Article 1710. https://doi.org/10.1186/s40064-016-3358-z.

[16] S. Bazm, P. M. Lima, and S. Nemati, Discretization methods and their extrapolations for two-dimensional nonlinear Volterra–Urysohn integral equations, *Applied Numerical Mathematics*, Vol. 208, 2025, pp. 323–337. https://doi.org/10.1016/j.apnum.2024.10.006.

[17] R. Rach, A convenient computational form for the Adomian polynomials, *Journal of Mathematical Analysis and Applications*, Vol. 102, No. 2, 1984, pp. 415–419. https://doi.org/10.1016/0022-247X(84)90181-1.

[18] W. B. Gragg, The Padé table and its relation to certain algorithms of numerical analysis, *SIAM Review*, Vol. 14, No. 1, 1972, pp. 1–62. https://doi.org/10.1137/1014001.

[19] P. Linz, *Analytical and Numerical Methods for Volterra Equations*, Studies in Applied and Numerical Mathematics, Vol. 7, SIAM, Philadelphia, 1985. ISBN (print): 978-0-89871-198-1. https://doi.org/10.1137/1.9781611970852.

[20] H. Brunner and M. D. Evans, Piecewise polynomial collocation for Volterra-type integral equations of the second kind, *IMA Journal of Applied Mathematics*, Vol. 20, No. 4, 1977, pp. 415–423. https://doi.org/10.1093/imamat/20.4.415.

Contribution of Individual Authors to the Creation of a Scientific Article (Ghostwriting Policy)

The authors equally contributed in the present research, at all stages from the formulation of the problem to the final findings and solution.

Sources of Funding for Research Presented in a Scientific Article or Scientific Article Itself

No funding was received for conducting this study.

Conflict of Interest

The authors have no conflicts of interest to declare that are relevant to the content of this article.

Creative Commons Attribution License 4.0 (Attribution 4.0 International, CC BY 4.0)

This article is published under the terms of the Creative Commons Attribution License 4.0 https://creativecommons.org/licenses/by/4.0/deed.en_US

APPENDIX

Table 1. Absolute error of the raw ADM partial sum for $\kappa = 1$; the $[0/1]$ Padé error is zero to machine precision in every entry.

$z = xt$	$n = 2$	$n = 4$	$n = 8$	$n = 12$
0.25	2.0833×10^{-2}	1.3021×10^{-3}	5.0863×10^{-6}	1.9868×10^{-8}
0.64	7.2818×10^{-1}	2.9826×10^{-1}	5.0040×10^{-2}	8.3953×10^{-3}
0.90	7.2900	5.9049	3.8742	2.5419

Source: created by the authors.

Table 3. ADM and Picard errors measured against the converged discrete solution of (35) with reference value $u_h(0.25, 0.25) = 0.525132196022$.

n	ADM error	ADM residual	Picard error	Picard residual
0	9.50720×10^{-3}	9.42400×10^{-3}	9.50720×10^{-3}	9.42400×10^{-3}
1	8.31939×10^{-5}	8.28473×10^{-5}	8.31939×10^{-5}	8.28473×10^{-5}
2	7.37236×10^{-7}	7.35558×10^{-7}	3.46609×10^{-7}	3.45766×10^{-7}
3	7.33111×10^{-9}	7.32029×10^{-9}	8.43332×10^{-10}	8.41983×10^{-10}
4	7.24376×10^{-11}	7.23619×10^{-11}	1.34848×10^{-12}	1.34693×10^{-12}
5	7.06435×10^{-13}	7.05873×10^{-13}	1.55431×10^{-15}	1.53003×10^{-15}
6	6.99441×10^{-15}	6.96838×10^{-15}	0	5.72459×10^{-17}

Source: created by the authors.

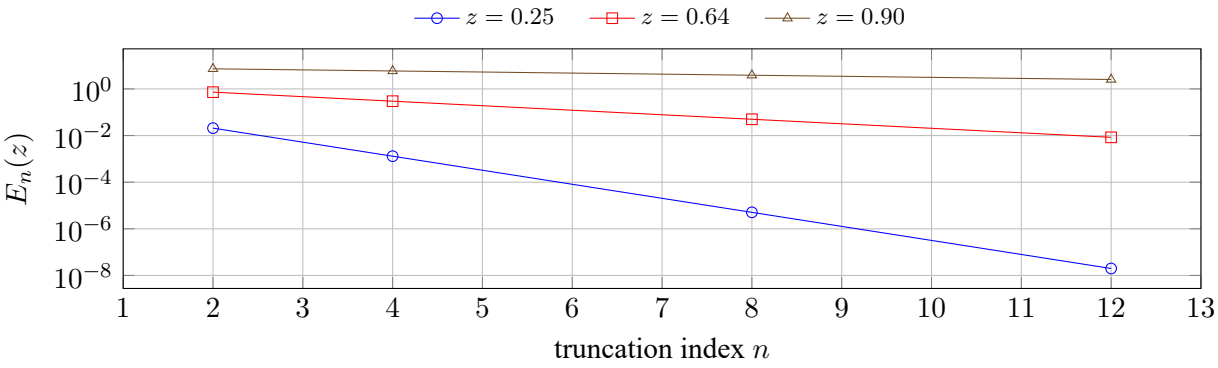

Fig. 1: Raw ADM truncation error for the blow-up benchmark. Proximity to $xt = 1$ controls the loss of convergence speed.

Source: created by the authors.

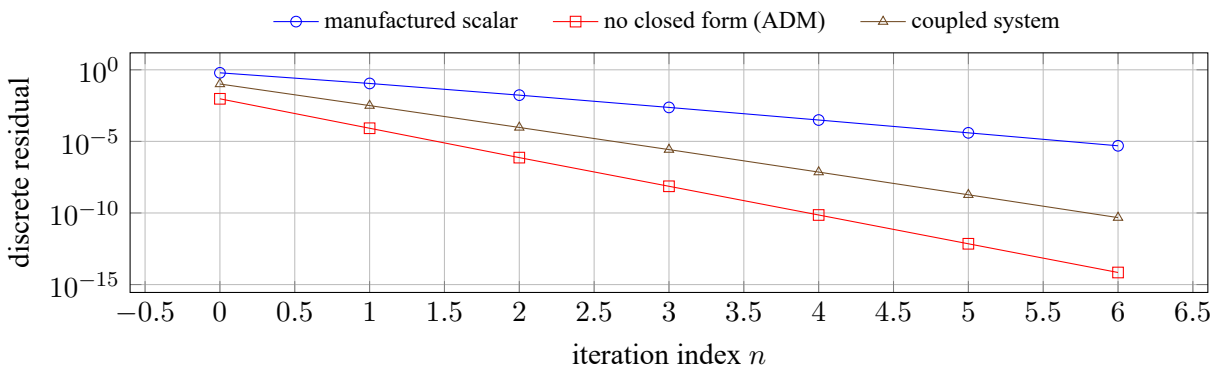

Fig. 2: Discrete fixed-point residuals by iteration index. The corresponding quadrature error floors appear in Table 2 and Table 5.

Source: created by the authors.